International Journal of Thermal Sciences 48 (2009) 1377–1391

Contents lists available at ScienceDirect

International Journal of Thermal Sciences

www.elsevier.com/locate/ijts

Flow and heat transfer characteristics in an annulus wrapped with a helical wire

T. Sreenivasulu, B.V.S.S.S. Prasad *

Department of Mechanical Engineering, IIT Madras, Chennai 600036, India

ARTICLE INFO

Article history:
Received 17 July 2008
Received in revised form 24 November 2008
Accepted 28 November 2008
Available online 7 January 2009

Keywords:
Flow and heat transfer
Cylindrical annuli
Helically wrapped wire
Hotspots
Augmentation
CFD

ABSTRACT

Convective heat transfer for an annulus, having its inner cylinder wrapped with a helical wire, has been numerically studied. Constant heat flux boundary condition is applied at the inner wall of the annulus whereas the outer wall is insulated. The computer code with *k*-omega SST turbulence model has been validated with the results of bare annulus. Several numerical results such as variations in velocity, pressure, vorticity, turbulent kinetic energy, temperature, friction factor and Nusselt number are presented for various annulus diameter ratios ($D/d = 1.5$, 1.8 and 2.0), pitch ratios ($P/d = 9.09$, 18.18 and 30.30), wire diameter ratios ($D_w/d = 0.15$, 0.25 and 0.30) and Reynolds number ($Re = 20000$ to 180000). The zones of possible hot-spots in the cusp region close to the wrap-wire are discerned.

1. Introduction

Heat transfer augmentation is attempted in many industrial heat exchange devices, nuclear rod bundles and process equipment. Cylindrical annulus is often considered as model geometry for practical heat exchanger devices and therefore thermal hydraulic investigations for the annular geometry are considered basic. Helically wrapped wires are introduced around the fuel rods of nuclear reactors for thermo-mechanical reasons; i.e. to act both as heat transfer enhancer and a structural stabilizer. As the wire produces a flow field with a circulatory motion, the swirling fluid in turn improves the transport rate. The annulus, helically wrapped with wire, may be conceived as a general heat transfer augmentation device.

A large body of literature is available on bare cylindrical annuli. Whilst analytical studies are available mainly in the laminar regime [1], experimental investigations on turbulent flow through the cylindrical annuli date back to 1930's [2]. Empirical correlations for friction factor and Nusselt number covering wider ranges of turbulent flow conditions and diameter ratio continue to be reported [3–9]. The most recent survey on bare cylindrical annuli is given in [9]. From the review of literature, however, it is evident that there is a wide variation in the published heat transfer data, as summarized in Fig. 1.

There are both computational and experimental studies [10–15] available on thermal-hydraulics in helical wire/tape inserted inside the tubes. The main purpose of these investigations is to determine the increase in friction factor and overall heat transfer in pipe flows due to these augmentation devices. However, by the insertion of helical wire into the cylindrical annulus, the flow field is locally distorted in the annulus. This may cause augmentation in some regions, but may also trigger hot spots at some other locations. If the hot spot temperature reaches an unacceptable value,

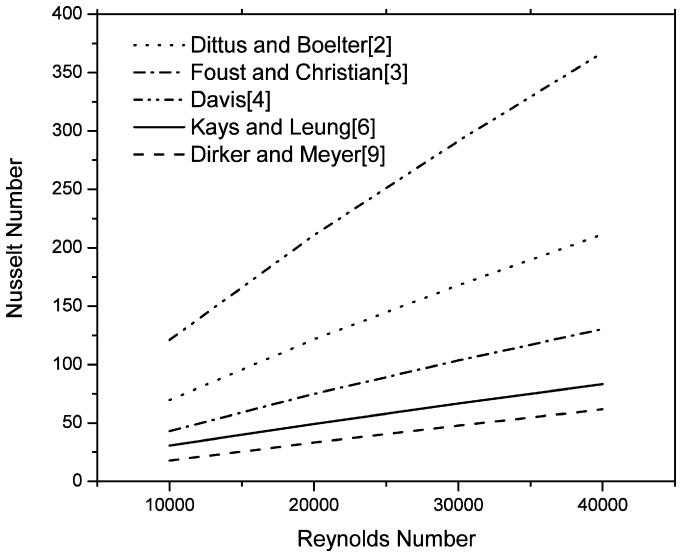

Fig. 1. Nusselt number correlations reported in [9] for turbulent flows in cylindrical annuli.

* Corresponding author. Tel.: +91 44 2257 4671; fax: +91 44 2257 4652
E-mail addresses: chittoorreddy@gmail.com (T. Sreenivasulu), prasad@iitm.ac.in (B.V.S.S.S. Prasad).

1290-0729/$ – see front matter
doi:10.1016/j.ijthermalsci.2008.11.023

Nomenclature

D	outer diameter	m
D_ω	cross diffusion term in turbulence	
d	inner diameter	m
p	pressure	Pa
E	energy	J/kg
f	friction factor	
G	generation term of turbulence	
I	unit tensor	
K	thermal conductivity	W/m K
Nu	Nusselt number	
p	helical pitch length	m
q''	heat flux	W/m^2
Re	Reynolds number	
S	source term in turbulence	
T	temperature	K
V	velocity	m/s
x	local axial distance	m
Y	dissipation term in turbulence	
y^+	viscous grid spacing	

Greek symbols

Δ	difference	
κ	turbulent kinetic energy	m^2/s^2
μ	dynamic viscosity	Pa s
Ω	vorticity magnitude	1/s
ω	specific dissipation rate	1/s
ρ	density	kg/m^3
τ	shear stress	N/m^2
∇	gradient operator	

Subscripts

average	average magnitude
axial	axial component magnitude
h	hydraulic
in	inlet
local	local magnitude
max	maximum
rad	radial component magnitude
tan	tangential component magnitude
w	wrap-wire
κ	turbulent kinetic energy
ω	specific dissipation rate

Abbreviations

SDR	specific dissipation rate
TKE	turbulent kinetic energy
THPR	thermo hydraulic performance ratio

the life of the tube may be reduced. There was no report of previous work on the thermal hydraulic in annuli with helical wire as insert, describing the local variations of flow and thermal characteristics and consequent formation of hot spots.

As the wire is introduced into the annulus, several parameters like tube to wire diameter ratio, the wire-pitch to diameter ratio come into play. The parametric investigation through experimental methods in the wire-wrapped annuli is quite expensive and difficult. Therefore, a numerical investigation is launched to study the thermal hydraulic behavior of fluid flowing through a wire-wrapped annulus. The parametric influences of varying Reynolds number (Re) range: 20000 to 180000, outer diameter to inner diameter ratio (D/d) range: 1.5 to 2, wire diameter to inner diameter ratio (D_w/d) range: 0.15 to 0.30 and pitch to inner diameter ratio (P/d) range: 9.09 to 30.3 are computationally investigated in this paper.

2. Physical model and meshing

The physical configuration and computational domain in Fig. 2 is a concentric cylindrical annulus with a wire wrapped around the inner cylinder. Different physical models are considered in accordance with the chosen parametric variations. In order to obtain the numerical solution, the annular domain is discretized by automatic mesh generation tools.

The bare annulus model is used for the purpose of validating the computational methodology. The overall length of the annulus is taken to be one-hundred times the hydraulic diameter. A mesh containing hexahedral cell volumes is first generated for the annulus without the wrap-wire as shown in Fig. 3. A fine clustered mesh is generated near the wall regions to yield a maximum wall y^+ not to exceed 4 at the inner wall. The mesh size for the bare annuli which is used for validation is chosen as 0.35 million after the grid independence study with mesh size varying from 0.12 to 1.2 million cells.

The cusp contact between the wire and inner cylinder is an inherent problem for generating a good mesh in the helical wrap-wire annulus. The complexity arises due to the presence of helical edge contact, formed between the wrap-wire and the inner cylinder. This problem is ameliorated by approximating the helical edge contact with a helical plane contact, having a width of $0.036D_w$ as shown in Fig. 4. This value of contact plane width is arrived at after several trials, essentially as a compromise between the desirable (line contact) and the attainable plane contact accuracy. Similar procedure for bare annuli is adopted to obtain a fine clustered mesh with y^+ less than 4 after several trails. A typical hexahedral mesh is thus generated as shown in Figs. 5 and 6. The total numbers of grids used finally for computation are shown in Table 1 for typical geometric variation.

3. Methodology

The differential equations governing the flow, turbulence and heat transfer under the assumptions of steady, incompressible flow are given as follows:

Conservation of mass:

$$\left(\nabla.(\rho\vec{v}) = 0\right) \tag{1}$$

Conservation of momentum:

$$\nabla.(\rho\vec{v}\vec{v}) = -\nabla p + \nabla.(\bar{\bar{\tau}}) + \rho\vec{g} \tag{2}$$

The stress tensor $\bar{\bar{\tau}}$ is given by

$$\bar{\bar{\tau}} = \mu\left[(\nabla\vec{v} + \nabla\vec{v}^T) - \frac{2}{3}\nabla.\vec{v}I\right] \tag{3}$$

Where the second term on the right-hand side is the effect of volume dilation. For incompressible flow, $[\nabla.\vec{v}I]$ becomes zero.

Conservation of energy:

$$\nabla.\left(\vec{v}(\rho E + p)\right) = \nabla.\left(k_{\text{eff}}\nabla T - \sum_j h_j\vec{J}_j + \left(\overline{\overline{\tau_{\text{eff}}}}.\vec{v}\right)\right) \tag{4}$$

Where k_{eff} is the effective conductivity $= k + k_t$, k_t is the turbulent thermal conductivity, defined according to the turbulence model

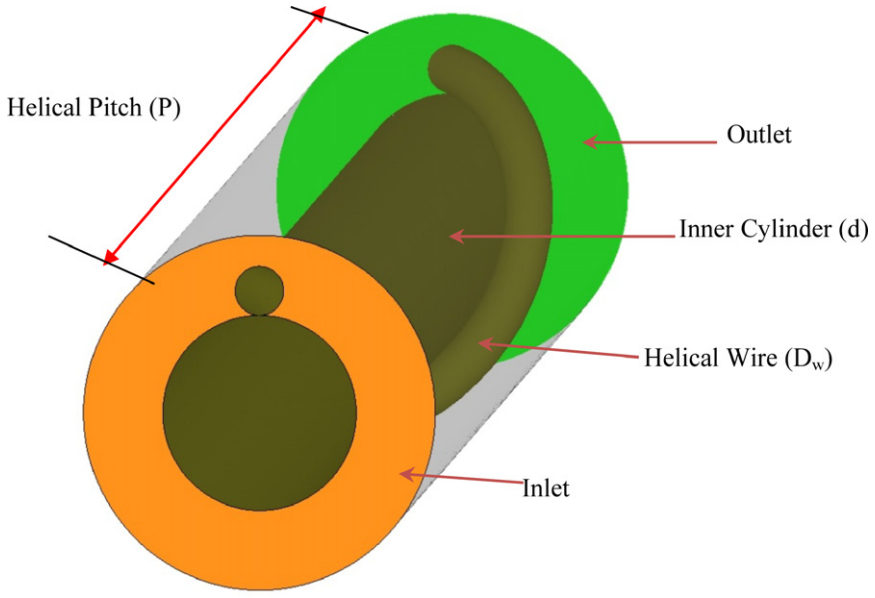

Fig. 2. Physical model of annulus with wrap wire.

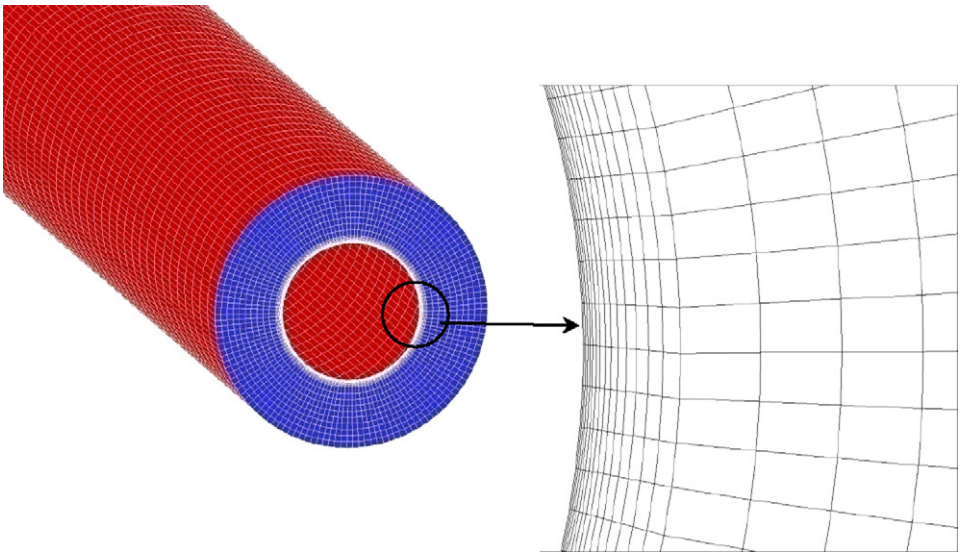

Fig. 3. Hexahedral mesh with clustering of grid near walls for bare annulus.

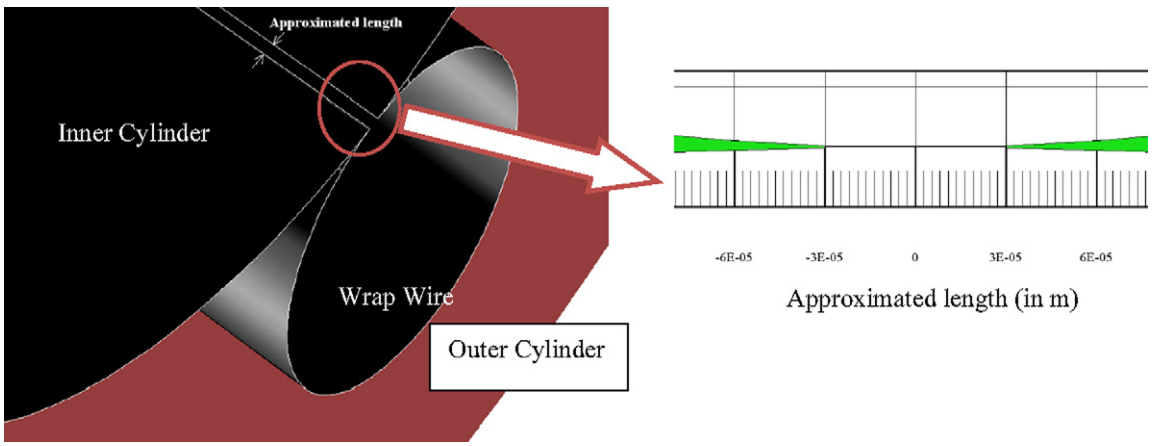

Fig. 4. Geometry showing cusp contact between the cylinder and the wire wrap.

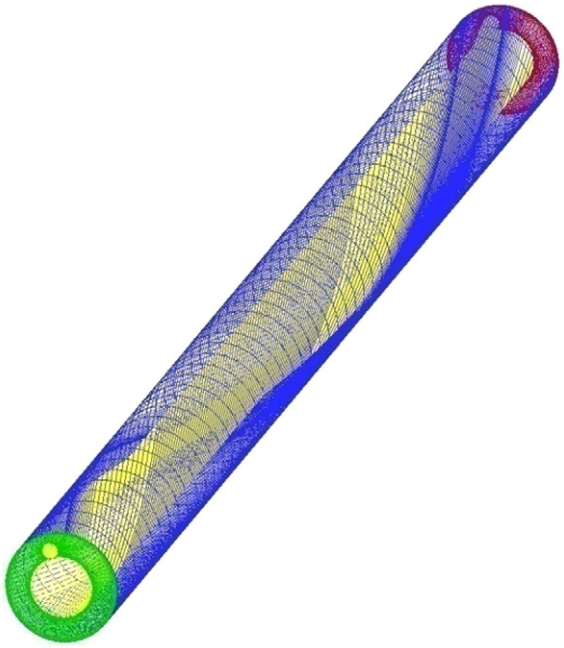

Fig. 5. Hexahedral mesh with clustered mesh near walls.

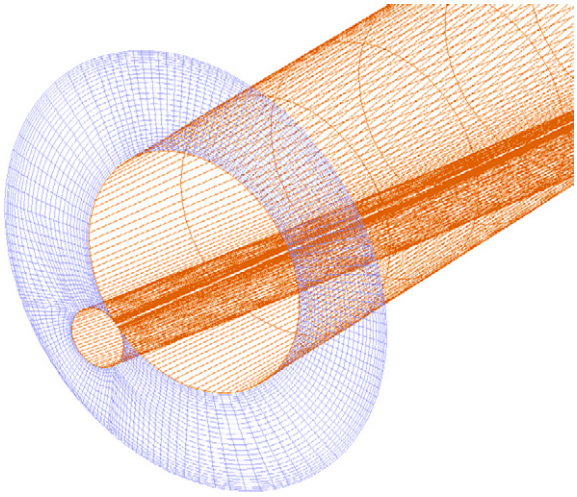

Fig. 6. Zoomed view of annulus with helical wrap wire.

Table 1
Mesh size and maximum wall y^+ of Inner wall for different configurations.

Configuration			Mesh size	Maximum wall y^+ for inner wall
D/d	P/d	Dw/d		
2.0	30.30	0.25	186550	2.09
1.8	30.30	0.25	186550	2.13
1.5	30.30	0.25	171850	4.85
1.8	18.18	$P/d = 18.18$	111930	2.29
1.8	9.09	$P/d = 9.09$	55965	2.29
1.8	30.30	$Dw/d = 0.15$	186550	2.23
1.8	30.30	$Dw/d = 0.3$	186550	2.03

being used. The first three terms on the right-hand side of Eq. (4) represent energy transfer due to conduction, species diffusion, and viscous dissipation respectively.

TKE equation:

$$\frac{\partial}{\partial t}(\rho\kappa) + \frac{\partial}{\partial x_i}(\rho\kappa u_i) = \frac{\partial}{\partial x_j}\left(\Gamma_\kappa \frac{\partial \kappa}{\partial x_j}\right) + G_\kappa - Y_\kappa + S_\kappa \quad (5)$$

SDR equation:

$$\frac{\partial}{\partial t}(\rho\omega) + \frac{\partial}{\partial x_i}(\rho\omega u_i) = \frac{\partial}{\partial x_j}\left(\Gamma_\omega \frac{\partial \omega}{\partial x_j}\right) + G_\omega - Y_\omega + D_\omega + S_\omega \quad (6)$$

Where $\Gamma_\kappa = \mu + \frac{\mu_t}{\sigma_\kappa}$, $\Gamma_\omega = \mu + \frac{\mu_t}{\sigma_\kappa}$, $\sigma_{\kappa,1} = 1.176, \sigma_{\omega,1} = 2.0, \sigma_{\kappa,2} = 1.0, \sigma_{\omega,2} = 1.168$.

The overall methodology used in present analysis is given in Fig. 7 in the form of Flow chart which is self explanatory. All these equations are solved using Fluent (Version 6.3) finite volume commercial code. Implicit first order upwind scheme is used for solving the above equations. The convergence criterion is fixed such that the residual values are lower than 10^{-6}. The pressure correction approach using the SIMPLE algorithm is used. Mass flow rate is specified at the inlet whereas static pressure is given at the outlet. Static temperature of the fluid (ambient value) is specified at the inlet. These input conditions are estimated indirectly from the chosen Reynolds number value. An adiabatic and no slip wall boundary are assumed for the outer wall of the annulus. Uniform heat flux condition is applied for the outer wall of the inner cylinder. The temperature difference between surfaces of helical wire and the inner cylinder are assumed to be negligible. This means that a conjugate analysis due to presence of conduction across the surfaces is not necessitated. Thus the same heat flux values imposed on inner cylinder are applicable for the helical wrap-wire surface as well. The turbulence model is chosen after applying various two-equation turbulence models available in the software. While all the turbulence models have yielded same results for bare annuli, the turbulence model has significant influence on the results of wire-wrapped annuli. It has been found by experimenting with different turbulence models, that the best model for good convergence is k–ω SST as it has predicted the flow in the wake of the cylinder very well. It is also evident from the literature [16] that k–ω SST is perhaps the best among the RANS models when flow field contains recirculation cells. In keeping with the above, the k–ω SST model is chosen for prediction of the turbulent flow hydrodynamics and transport rate in the annulus with wrap-wire.

4. Validation for bare annulus

For all the annular geometries, computations are carried out for various Reynolds numbers up to a uniform convergence criterion with the residuals lower than 5×10^{-12}. Nusselt number values at a length of 100 times the hydraulic diameter are plotted against Reynolds number. The Reynolds number range chosen is the same as of the correlations provided by Kays [6] and Dirker [9]. Comparison of these works is found to yield a fifteen percent deviation (Fig. 8) which is better than the general disagreement of various correlations available in the literature (Fig. 1). The predicted values by the present methodology are considered acceptable and hence the methodology is deemed to have been validated.

5. Results and discussion

5.1. Flow characteristics of typical wire wrapped annulus

The computed results of flow characteristics in the form of path lines velocity and pressure variations for the annulus without and with the wrapped wire are presented in Figs. 9 to 16. Figs. 9 (a) and (b) show the path lines for typical bare annulus ($D/d = 1.80$) and wire wrapped annuli ($D/d = 1.80$, $P/d = 30.30$, $D_w/d = 0.25$) respectively. The inner diameter is kept constant for all the geometries for which the results are presented in the present analysis. The extent of flow distortion from a straight undisturbed flow (Fig. 9(a)) to the highly skewed flow (Fig. 9(b)) due to the presence of helical wire is amply evident from these figures. The path

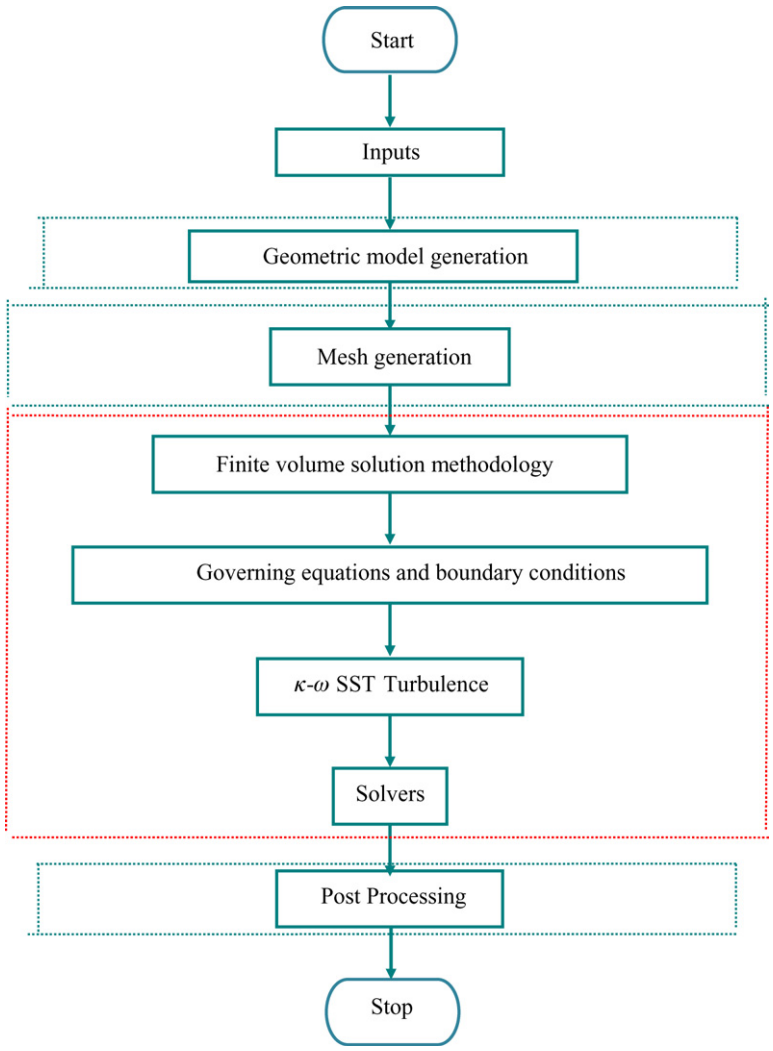

Fig. 7. Flow chart for over methodology used present analysis.

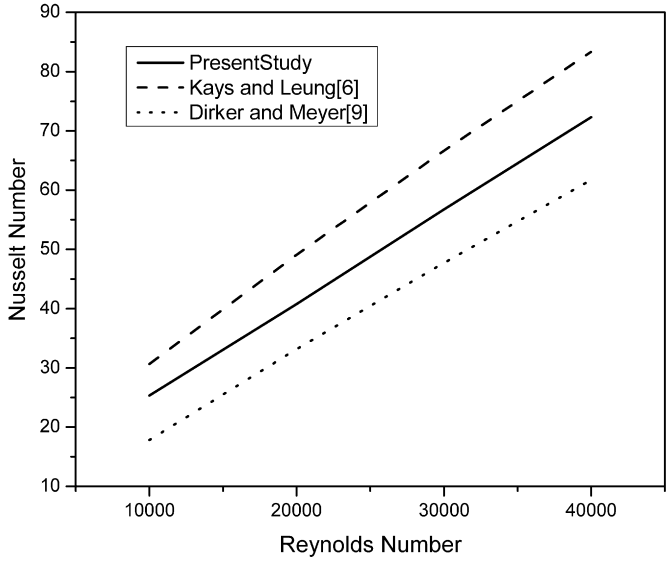

Fig. 8. Validation of present methodology.

lines depicted at a plane $x/p = 0.5$ (Fig. 9(c)) also show the qualitative influence that the wire has on the annular flow. The velocity of flow which is primarily axial in bare annulus, see Fig. 10(a), will have significant radial and tangential contributions in the wire-wrapped annulus, as shown in Figs. 10 (b), (c) and (d). Referring to Fig. 10(b), it is observed that the variation in the axial velocity components does not markedly change with respect to the position of wire. However, the variations in the radial and tangential components with reference to the position of the wire are significant along the annulus length as noted from Figs. 10 (c) and (d). The maximum swirl (the tangential velocity component) is about 12% of the mean velocity.

The velocity contours at $x/p = 0.5$ are shown in Fig. 11(a). The velocity near the wire is higher in front side compared to aft side as the wire is wrapped in a left hand helical screw fashion. The stagnation zone near the cusp region is amplified and shown in Fig. 11(a). Though there is asymmetry in the velocity contour in front and aft sides of wire, there is symmetry near the cusp region. The corresponding pressure variations at the same plane are drawn in Fig. 11(b). There is low pressure at the front side of the wrapped wire where the velocity is high. The reason for this variation in the mid plane can be explained from Fig. 9(c) where the path lines viewed on the plane ($x/P = 0.5$) clearly show the swirl due to insertion of wrapped wire annuli. Further there is a cross flow over the wire in the gap between the outer cylinder and the wire. Fig. 11(c) shows the contours of vorticity ratio and Turbulent Kinetic Energy (TKE) ratio presented back to back. The generation of vorticity is due to shear and swirl of the fluid in the gap between the wire and the outer cylinder. The vorticity generated in

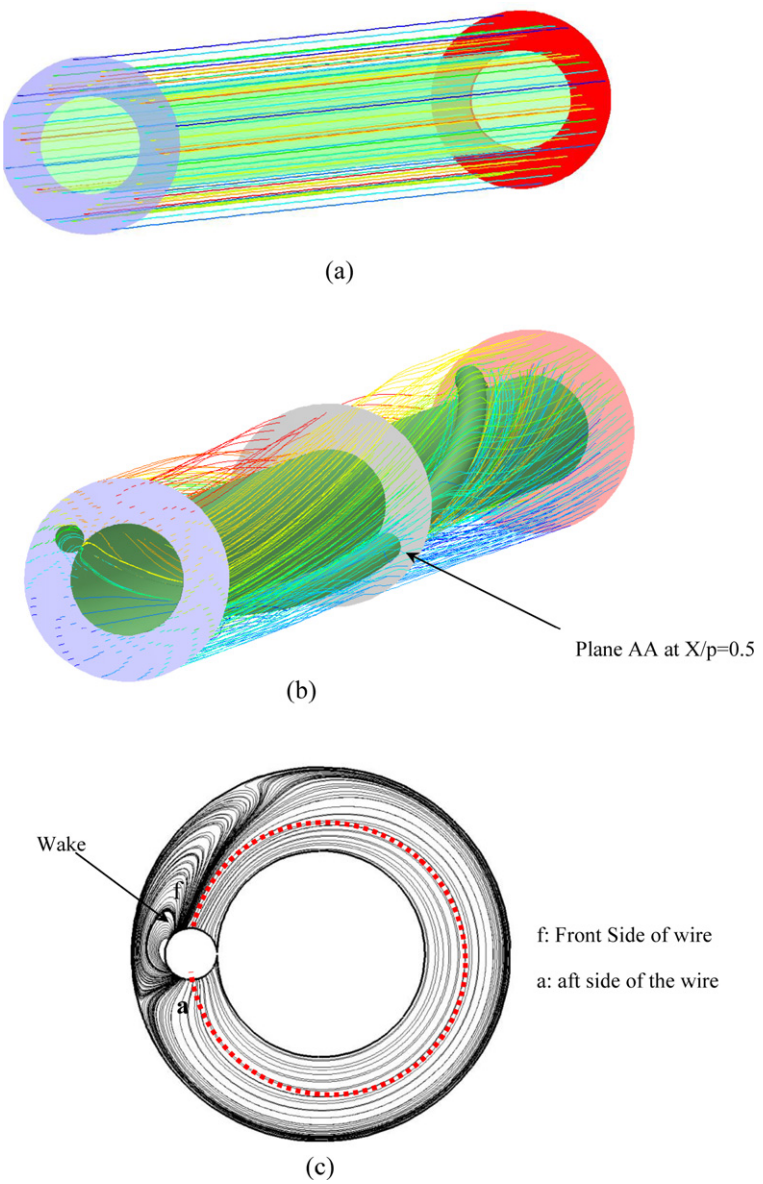

Fig. 9. Pathlines for (a) bare annulus, (b) helical wrapped wire annuli, and (c) wire-wrapped annuli at plane AA.

the gap is thus relatively high. The vorticity is higher in the front side compared to the aft side of the wire. It is evident from Figs. 11 (a) and (b) that the increase in TKE is qualitatively similar to the variation in the vorticity magnitude. The increase in TKE is one of the reasons for increase in heat transfer due to insertion of wire, which will be discussed in the later section.

Thus, whilst Fig. 11 gives a qualitative picture of the velocity and pressure variations, Figs. 12 and 13 compare these variations quantitatively for the bare and wire-wrapped annuli in the form of the polar plots. The data for these figures is taken at an axial location $x/p = 0.5$ (see plane AA in Fig. 9(b)). The radial location is at the mid of wrapped wire as denoted by the dotted line in Fig. 9(c). The scales in Figs. 11 and 12 indicate the magnitudes of the local velocity to average velocity ratio and the local pressure to average pressure ratio represented along the radial lines.

The velocity distributions for the bare annuli of all D/d ratios, when normalized with average velocity, fall on a single closed circular line, curve A, refer Fig. 12. However, because of the presence of wrap-wire, the velocity distribution becomes non-circular, curve B. The break in curve B is due to the presence of wire. The velocity distribution with wire-wrap (curve B) closely follows the velocity of bare annulus (curve A) from 0° to 110°. The variation between the two curves is not significant because the contribution to radial and tangential components between 0° and 120° is not substantial. The presence of wire is felt more strongly between 120° and 190°, where the velocity is much lower than the value for bare annulus. On the wall of the wire, the velocity becomes zero due to no-slip, but there is asymmetry in the velocity values in the front and aft sides of the wire. Fig. 13 shows the corresponding curves (A and B) for pressure variation. The above mentioned asymmetry in the velocity field can be observed better from these pressure curves. The pressure in the front side is high whereas it is low in the aft side; as noted from in Fig. 13.

Figs. 14 (a), (b) and (c) show the polar plots of the magnitudes of axial, tangential, and radial velocity variations for both the bare annulus and the wire-wrapped annuli of different D/d. It may be noted that the axial velocity profile (Fig. 14(a)) is almost same as the velocity magnitude in Fig. 11, for the curves (C, D) corresponding to $D/d = 1.8$ and 2.0. This is because; the contribution due to radial and tangential components is zero for all the bare an-

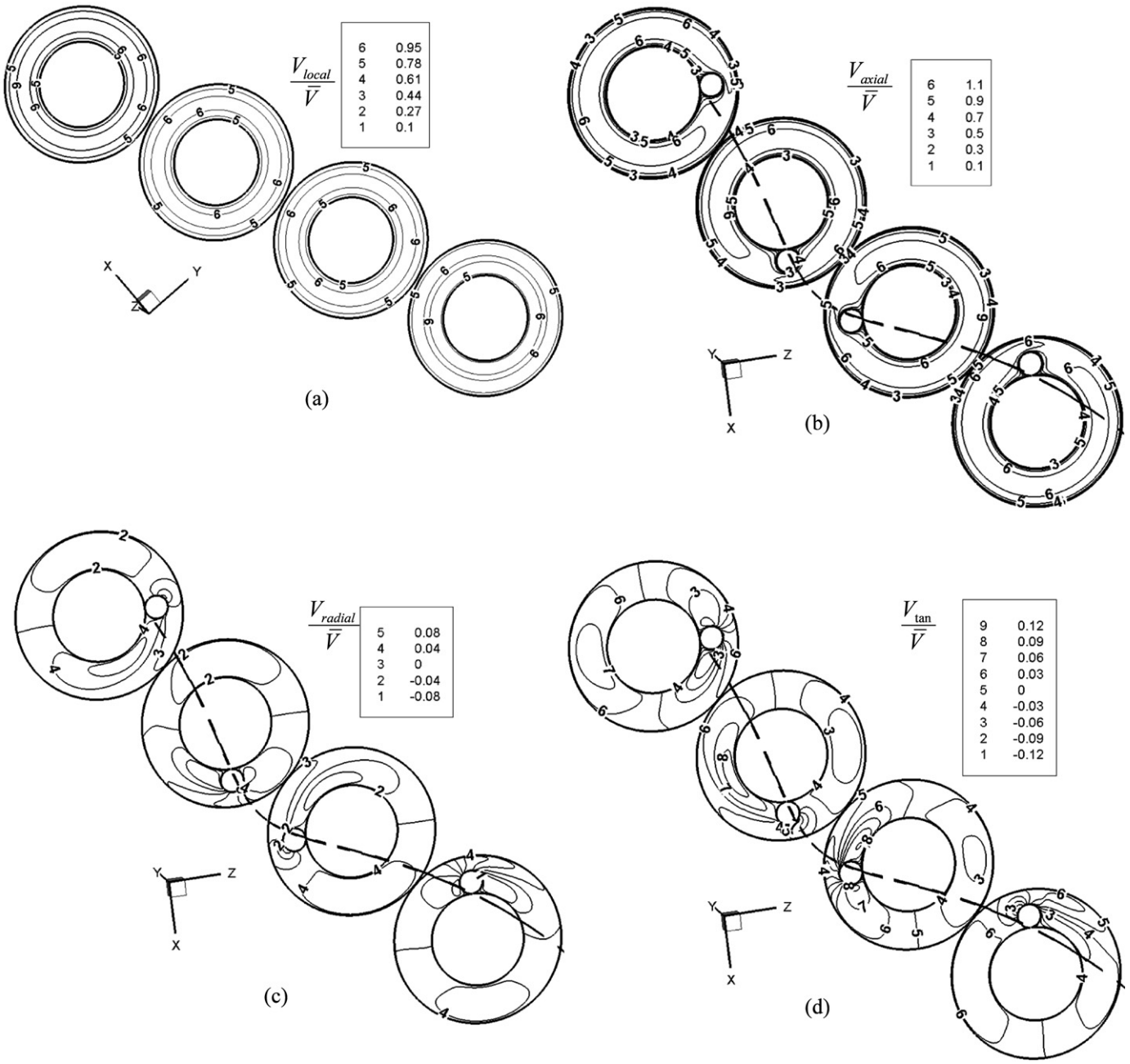

Fig. 10. Comparison of velocity contours for bare and wire wrapped along length. (a) Velocity magnitude contours in bare annuli, (b) axial, (c) radial, (d) tangential velocity variation in the wire wrapped annuli.

nuli and small for D/d value of 1.8 and 2.0. However, as the wire touches the outer tube, $D/d = 1.5$ (curve B) the axial component reduces significantly and the tangential and radial components increase as indicated in Figs. 14 (b) and (c). Figs. 11(c) and 15 (a) and (b) qualitatively show the extent of swirl with change in D/d, through the vorticity magnitude. These three figures bring out the effect of D/d on the generation of vorticity and TKE in the annulus. As the value of D/d decreases, velocity of swirl and values of the vorticity as well as TKE increase. At $D/d = 1.5$, the wire is symmetrically placed in the annulus whilst the cross flow is completely absent. This induces a symmetric pattern in the vorticity as well as TKE contours. As the swirl produced is large, the vorticity and TKE are also large.

The effect of D/d on the velocity and pressure variations for wire-wrapped annuli is shown in Figs. 16 (a) and (b). The velocity magnitude increases with decrease in the diameter. The distortions in velocity profile near the wire also increase with reduction in D/d. Unlike the velocity variation, the pressure difference between the front and aft sides of the wire increases with decreasing gap between the diameters, i.e. with decreasing D/d.

The changes in velocity profile for different values of pitch to diameter ratio are shown in Fig. 17(a). The decrease in pitch ratio causes an increase in swirl which in turn results in the increased resistance to flow. The corresponding changes in pressure can be noted from Fig. 17(b).

The changes in velocity and pressure distributions for different helical wire diameter to inner diameter ratios (D_w/d) are shown in Figs. 18 (a) and (b). The non-uniformity in velocity profile increases with the increase in wire diameter. The effect of cross flow is to increase the radial and tangential components of velocity. The

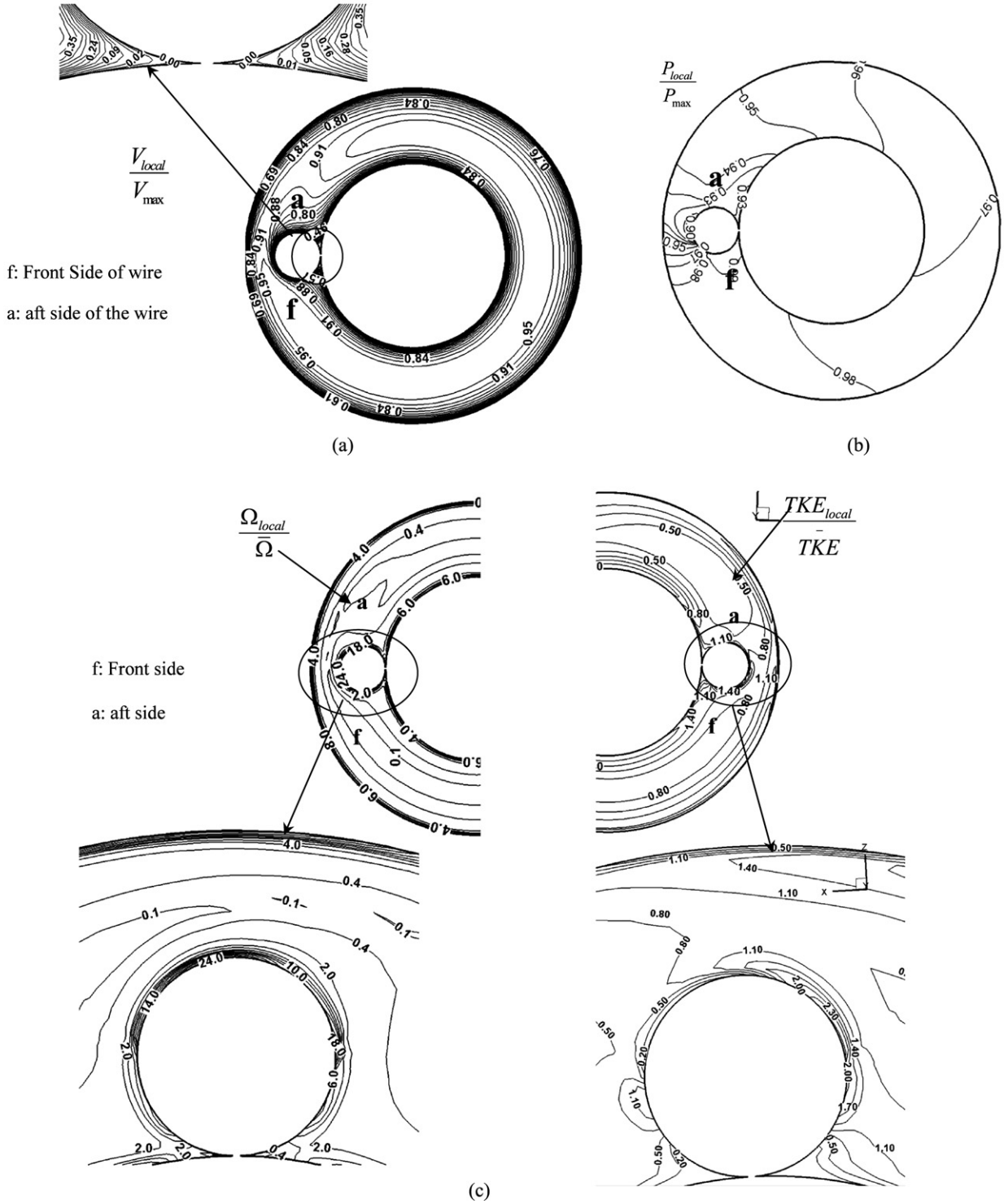

Fig. 11. Contours for wire wrapped annuli ($p/d = 30.3$, $D/d = 1.8$, $D_w/d = 0.25$). (a) Velocity, (b) pressure, (c) vorticity & TKE.

cross flow is clearly dependent on the wire diameter. The change in vorticity magnitude due to increased wire diameter is shown in Figs. 19 (a) and (b). It is evident that with smaller diameter wire the cross flow velocities are smaller and hence smaller are the vorticity and TKE generated.

The foregoing calculations are repeated for three different inner diameters, while keeping D/d constant. But in those cases, the values of p/d and d_w/d also changed. After considerable scrutiny of these data with the help of trends observed in Figs. 16 to 18, it could be concluded that there was no influence of the actual size of inner cylinder, as long as the dimensionless ratios are maintained. However, in order to prove this fact numerically in the paper, one would have to do considerable number of computational experiments. Each set of calculation being computationally very intensive; such an elaborate exercise has not been attempted.

5.2. Temperature distribution and hot spots

As stated earlier, the temperature variations in the flow and on the inner wall are key results which are important to evalu-

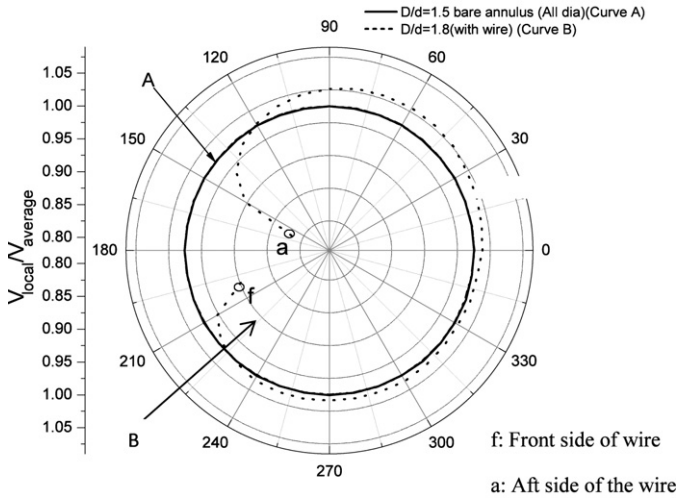

Fig. 12. Comparison of velocity profile with and without wire.

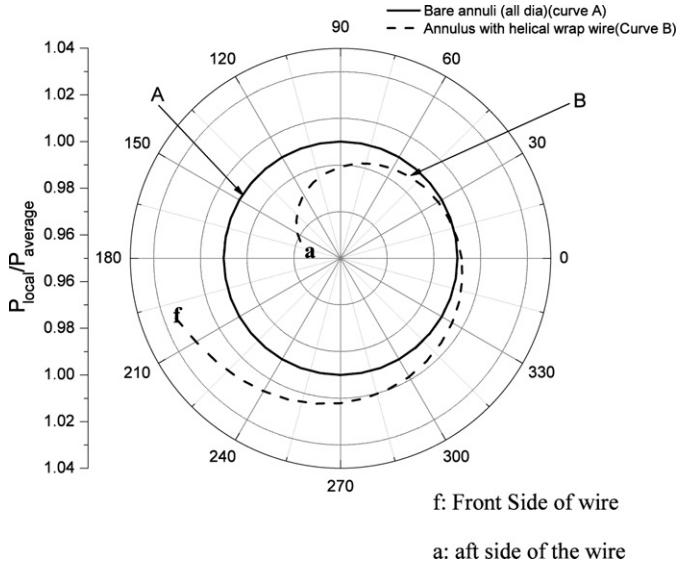

Fig. 13. Comparison of pressure profile with and without wire.

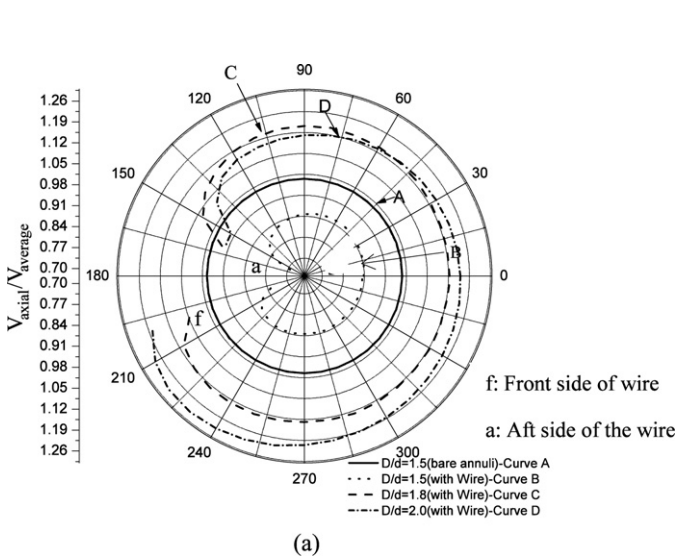

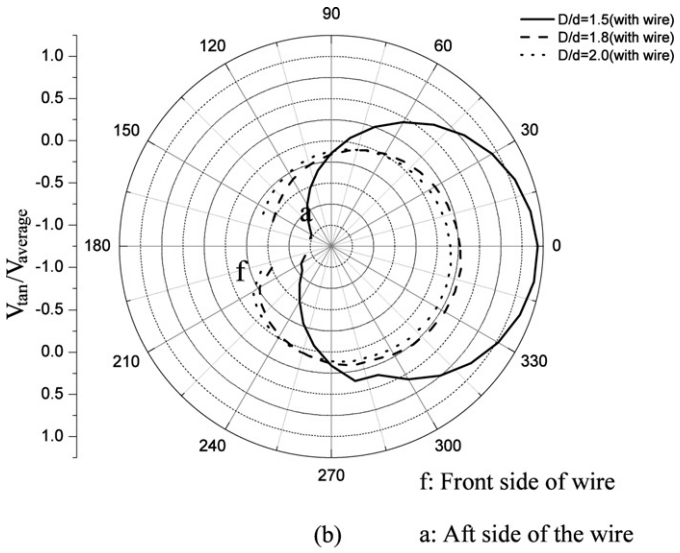

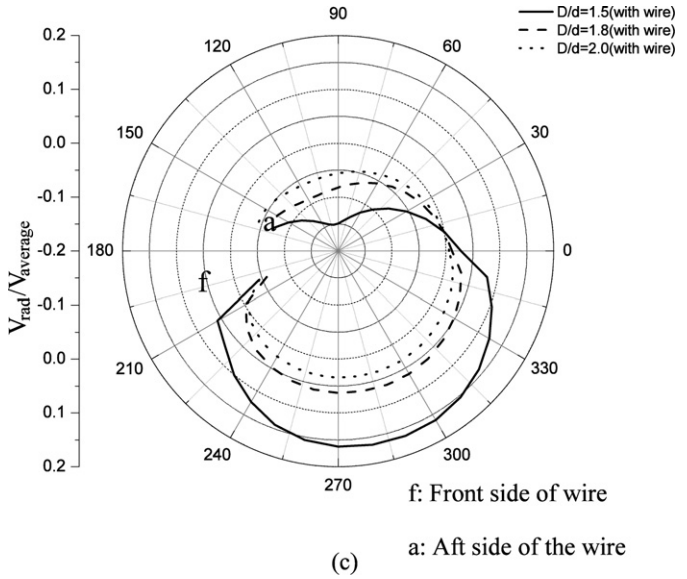

Fig. 14. Effect of diameter ratio (D/d) on (a) axial, (b) tangential, (c) radial velocities for $P/d = 30.30$, $D_w/d = 0.25$.

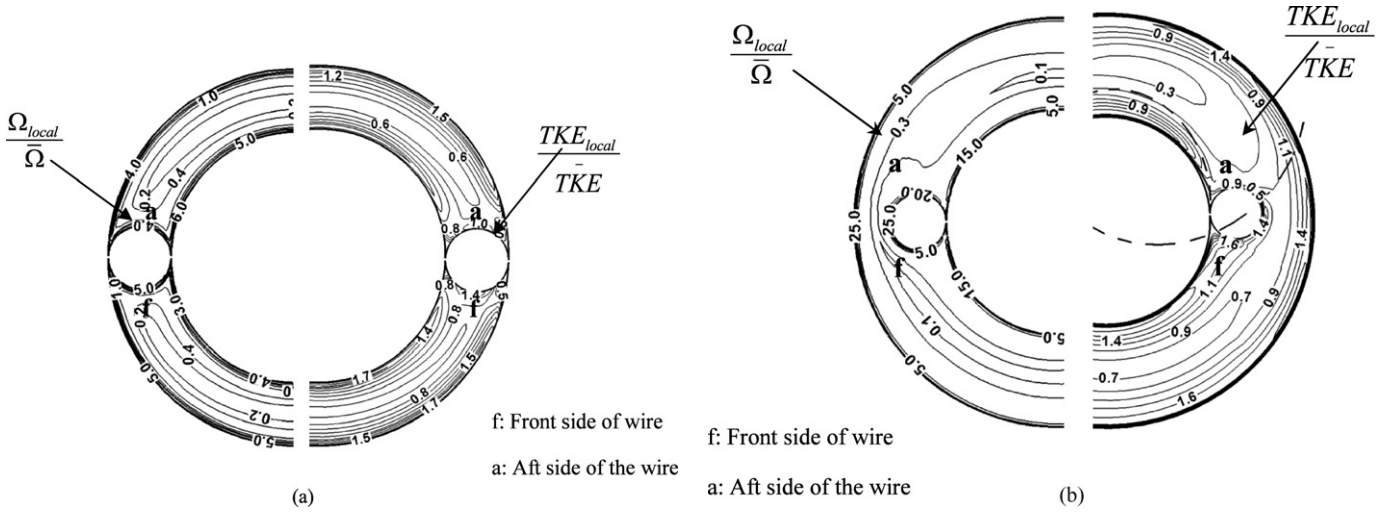

Fig. 15. Vorticity and TKE magnitude for the diameter ratios. (a) $D/d = 1.5$, (b) $D/d = 2.0$ for $P/d = 30.30$, $D_w/d = 0.25$.

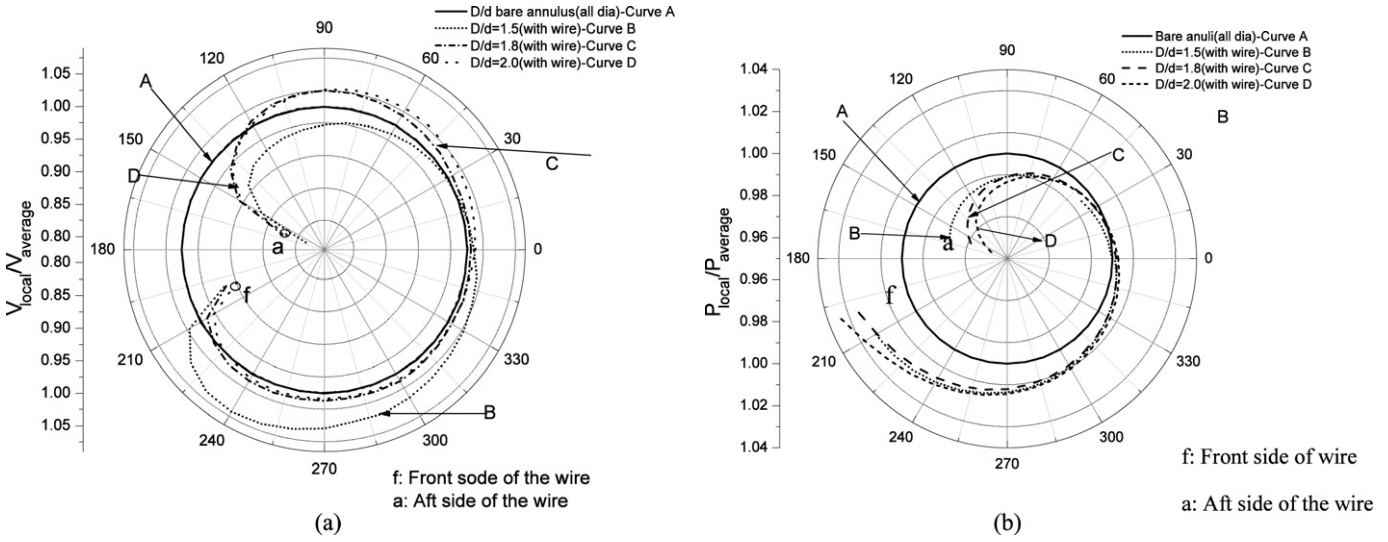

Fig. 16. Effect of diameter ratio (D/d) on (a) velocity, (b) pressure for $P/d = 30.30$, $D_w/d = 0.25$.

ate heat transfer characteristics and to cognize the hot spots that arise due to the presence of wire-wrap. Figs. 20 (a) and (b) compare the temperature contours of the wire-wrapped annulus with bare annulus for a uniform heat flux parameter ($q''L/k = 2383.33$) as input at the inner wall. The heat flux parameter is chosen such that fluid does not 'boil' close to the cusp region. Typically this value of heat flux parameter translates to a rate of specific enthalpy rise about 500 watts per meter length. With this input rate, Figs. 20 (a) and (b) show the contours of dimensionless temperature ratio (defined as $\theta = (T - T_{\text{in}})/(q''L/k)$) for the bare and the wire wrapped annuli respectively. Whilst the temperature contours are concentric circles for bare annulus they show asymmetry for the wire-wrapped annulus. It means more rise in temperature in the aft side than the front side of wire. Much closer to the wall, near to the cusp region, significant temperature variations up to 21% occurs. The cusp regions with high temperature gradients are important because phase change (if any) will be initiated here converting them to become critical hot spot zones. The value and extent of hot spot zone increases with increase in input heat flux and decrease in mass flow rate. Figs. 21 (a), (b) and (c) show the effect of D/d, P/d and D_w/d respectively on the temperature of inner wall. The data for these figures is taken at the inner cylinder. It is clear from these figures that near the stagnation zone of the cusp region, heat transfer is large but is low in its wake. The wall temperature distributions with wire-wrap (curves B, C, D) resemble the velocity variation for the bare annulus (curve A) closely from 0° to 130°. The variation between the two curves (say A and B) is not significant because the velocity in both of them is almost same as noted from Fig. 16(a). The presence of cusp region is felt between 130° and 230°, where the wall temperature is increased by more than 11% of the average temperature. Unlike the velocity profile (Fig. 12), the temperature profile is also symmetric in both front and aft sides of the wire. The variations in curve, A, B and C indicate that with decreasing D/d, the maximum wall temperature value decreases, increasing the heat transfer in that region due to increase in velocity. As p/d decreases (Fig. 21(b)) heat transfer increases very little although there is some increase in both surface area and velocity. However, there are significant changes in local temperature with change in wire diameter. The maximum temperature decrease as the wire size increases due to increase in surface area and velocity. Hence it is one of the important parameter for choosing an optimum geometric configuration.

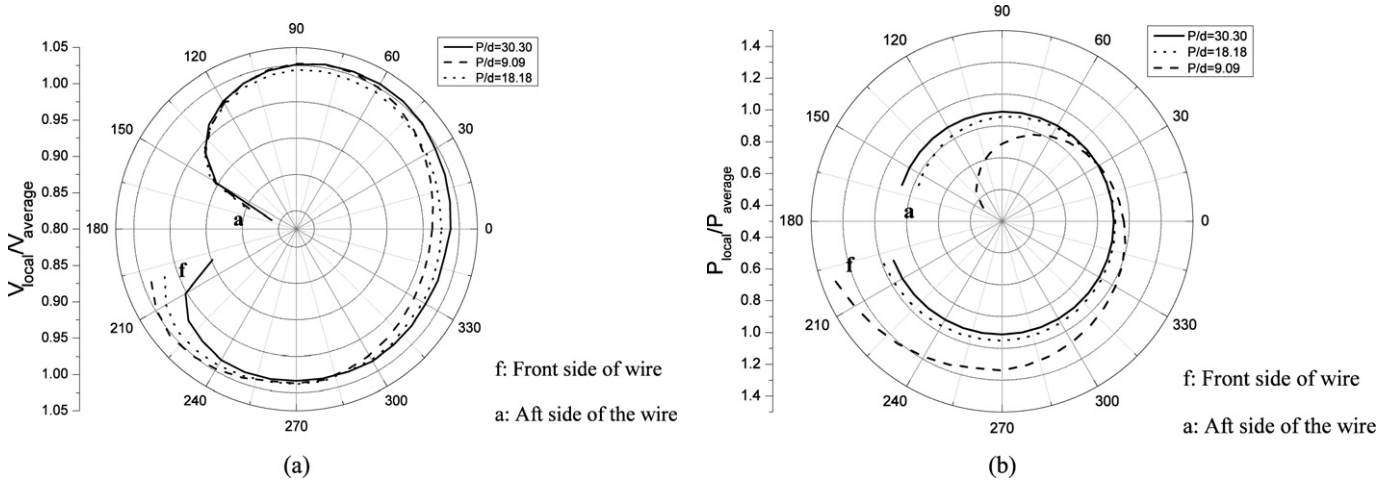

Fig. 17. Effect of pitch ratio (P/d) on (a) velocity, (b) pressure for $D/d = 1.8$, $D_w/d = 0.25$ for $D/d = 1.8$, $D_w/d = 0.25$.

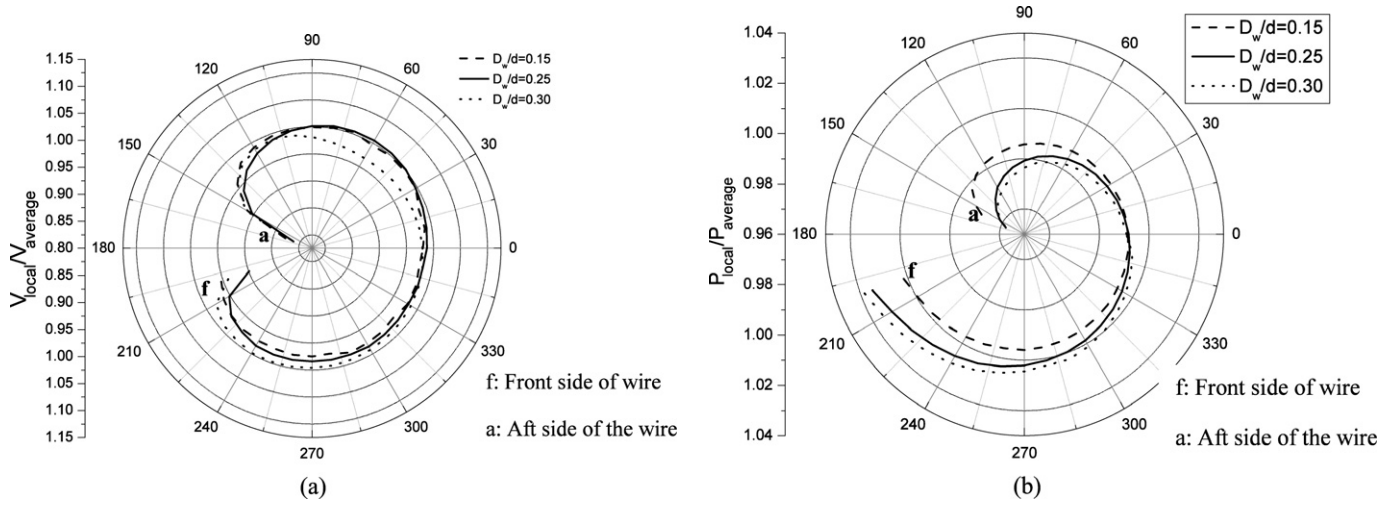

Fig. 18. Effect of wire diameter (D_w/d) on (a) velocity, (b) pressure for $D/d = 1.8$, $P/d = 30.30$.

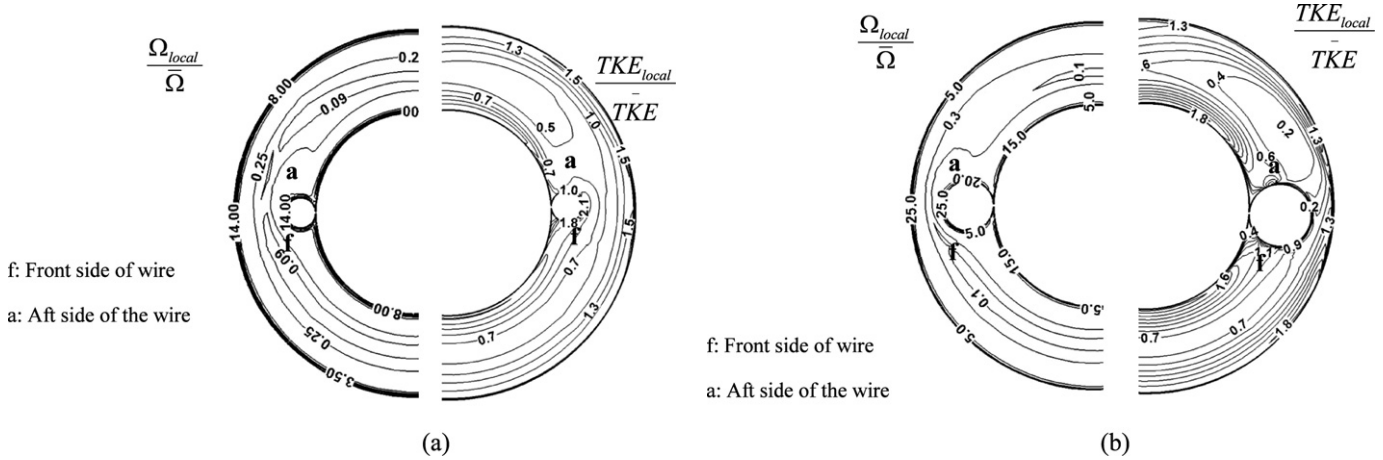

Fig. 19. Contour of vorticity and TKE for different wire diameters. (a) $D_w/d = 0.15$, (b) $D_w/d = 0.30$ for $D/d = 1.8$, $P/d = 30.30$.

5.3. Friction factor

The fanning friction factor is defined as $f = (2\Delta pd)/(\rho L v^2)$. As the velocity term appears in the denominator, increase in velocity due to the presence of the wire causes reduction in friction factor for small outer diameters. However, there will be an increase in pressure drop due to the wire wrap, which can be attributed to increase in tangential velocity (Fig. 14(b)). On the whole, the friction factor increases due to the presence of wire. The variations in the friction factor for different values of outer diameter ratios,

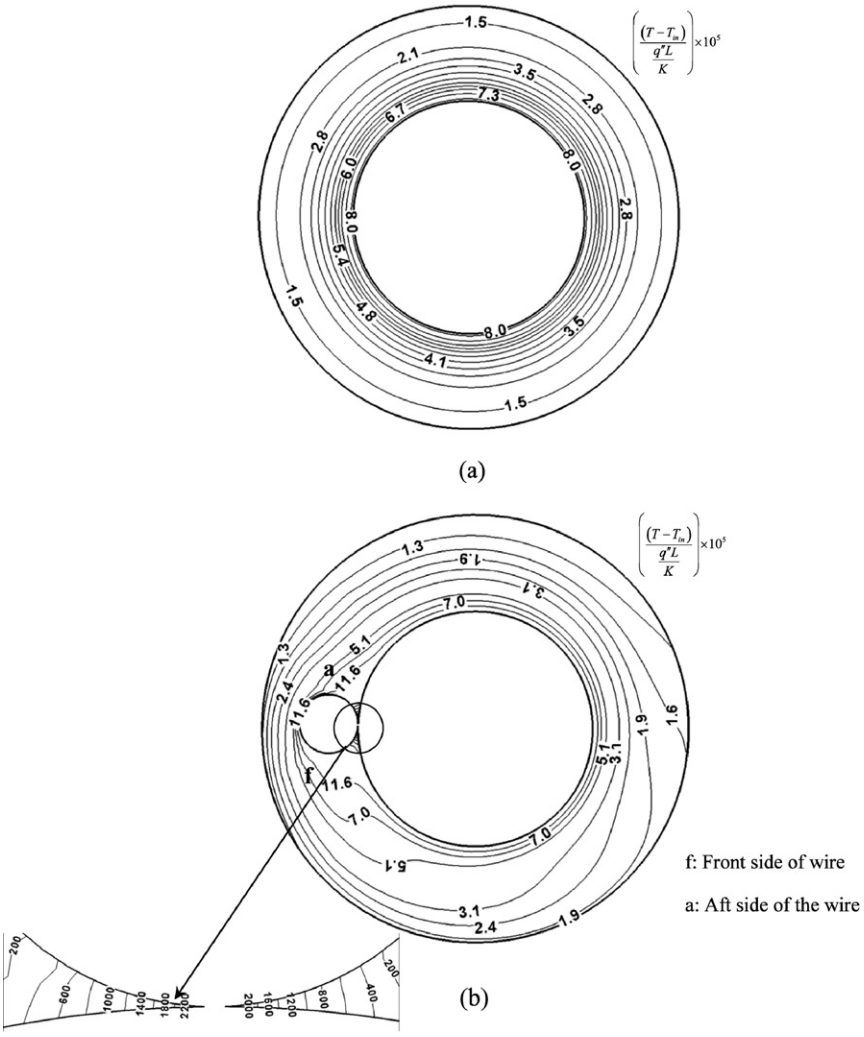

Fig. 20. Comparison of dimensionless temperature contours of (a) annulus and (b) wire for $P/d = 30.30$, $D_w/d = 0.25$.

pitch ratios, and wire diameter ratios are shown in Figs. 22 (a), (b) and (c) respectively. The variation of friction factor with increase in outer diameter and its comparison with bare annuli are shown in Fig. 22(a). The friction factor increases with increase in the outer diameter, even though the pressure drop itself decreases. The friction factor increases as the p/d (Fig. 22(a)) decreases. As the Reynolds number increases the friction factor starts to decrease. The slope of f vs. Re up to Reynolds number 0.5×10^5 is large compared to the slope after 0.5×10^5. The variation of friction factor with helical wire diameters is almost negligible; as seen from Fig. 22(c).

5.4. Nusselt number

The Nusselt number variations for bare and wire wrapped annuli with the Reynolds number varying from 20 000 to 180 000 shown in Fig. 23(a). As expected the heat transfer is increased with the introduction of wire. The change in Nusselt number is qualitatively in accordance with the *Nu* distributions for bare annulus at various Reynolds number. It is stated earlier that with the insertion of wire, the flow area decreases, velocity and its swirl as well as vorticity increase along with the turbulence generated. This swirl velocity induces centrifugal force near the inner wall of the wire wrapped annuli, which causes heat transfer enhancement. Another reason for the increase in convection heat transfer is the increase in turbulent mixing. Further, the exposed surface area also increases causing the enhanced heat transfer. The radius ratio of the wire wrapped annuli is varied by adjusting the outer diameter with fixed inner diameter and its effect is shown in Fig. 23(a). As the outer diameter is increased, the Nusselt number increases for a given Reynolds number. The change in the turbulence structure due to variation in annulus ratio is primarily responsible for such an interesting behavior. This variation of Nusselt numbers with D/d is experimentally shown by Dirker and Meyer [9]. The change in slope of *Nu* vs. *Re* can be attributed to drastic change in Reynolds number. There will be a rise in Nusselt number of around 300% at higher Reynolds numbers and for the lowest diameter ratio ($D/d = 1.5$), when compared with the result of bare annuli. The same curve, when it is compared with the wire wrapped annuli ($D/d = 2.0$), an increase of 22% is noticed for $D/d = 2.0$.

The variations in Nusselt number for different values of pitch are shown in Fig. 23(b). It is observed that the cases with lower pitch ratio have a higher Nusselt number and it reduces as the pitch ratio increases. This change in Nusselt number for variations in pitch observed here could be caused either due to the reduction in pitch length which results in reduction of overall annulus length, or due to reduction of helical pitch or both The increase in Nusselt number is also due to increase in turbulence intensity and swirl inflow. The increase in Nusselt number with the change in

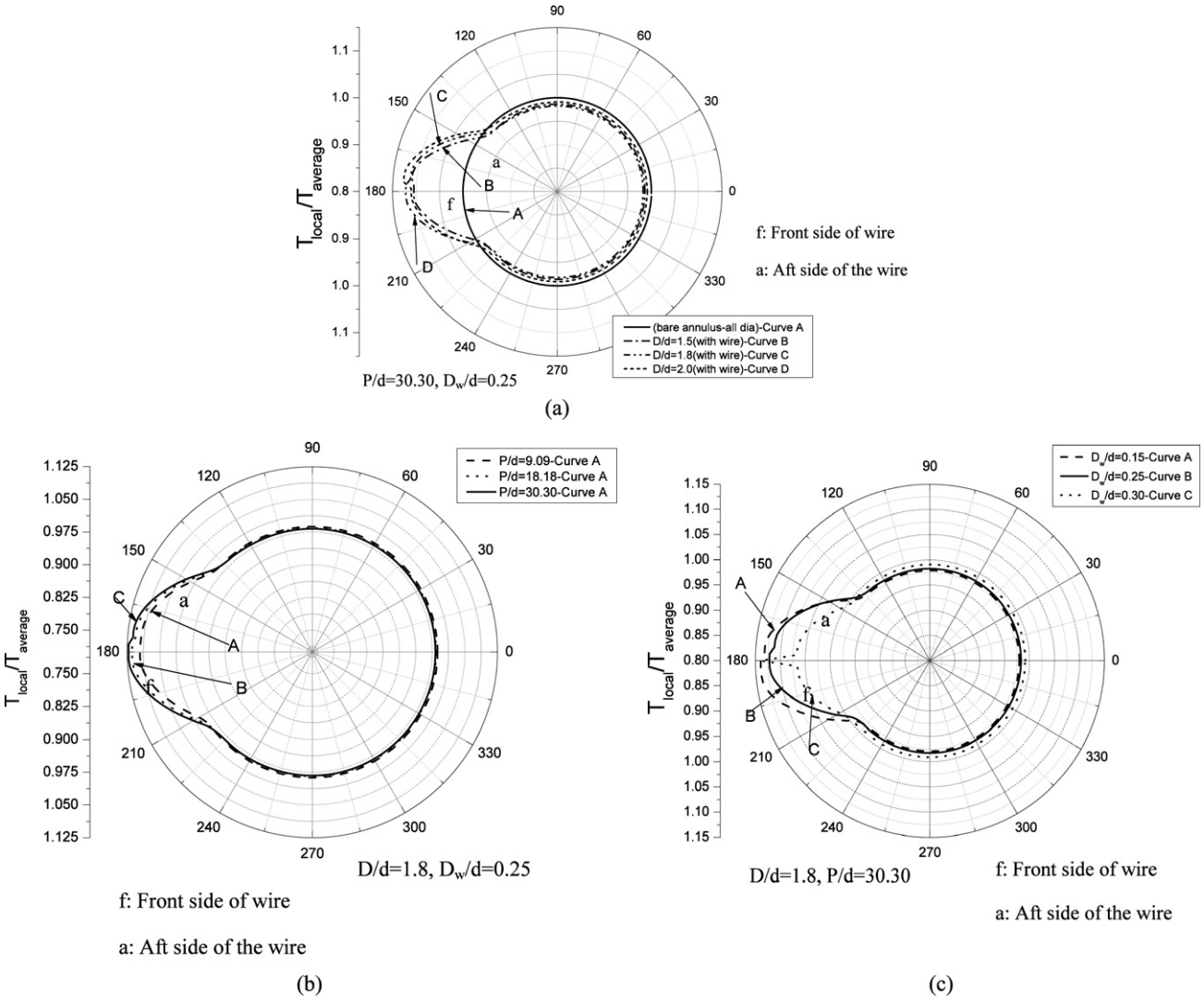

Fig. 21. Temperature variation for various (a) outer diameter (D/d), (b) pitch (P/d), (c) wire diameter (D_w/d).

the values of pitch from 9.09 to 30.3 at a nominal Reynolds number of 10^6 is around 20%.

Nusselt number variation for different wire diameters are shown in Fig. 23(c). The Nusselt number increases with the increase in wire diameter. As stated earlier, the increase in wire diameter causes the increase in velocity and the surface area, which inturn results in the increase of Nusselt number.

5.5. Performance

There is a large number of performance parameters in the literature to quantify the augmentation in heat transfer vis-à-vis pressure drop. In a recent paper [17], the ratio of heat transfer rate between enhanced and reference surfaces $((Nu_w/Nu)/(f_w/f))$ under identical flow rate are used as the performance parameter for quantifying the augmentation. This parameter is named as thermo hydraulic performance ratio, THPR. Fig. 24 shows the variation of THPR for various configurations with mass flow rate. It shows that the proposed configuration performs considerably better for all values of D/d, P/D and D_w/d. This figure may also help the designers to choose the parameters suitable to their application.

6. Conclusions

A computational study on convective heat transfer in an annulus with its inner cylinder wrapped by a helical wire is reported in this paper. The salient conclusions drawn from the study are:

1. The k–ω SST turbulence model is found to predict the flow and heat transfer characteristics satisfactorily.
2. The presence of wire in the annulus disturbs the flow, as a result of which the swirl component of velocity higher quantity of vorticity and turbulent kinetic energy are produced. These are responsible for increased transport rates in the annulus. The parameters D/d, P/d, D_w/d show the significant influence on the local transport rates.
3. In the cusp region close to the wrap-wire, there is a possibility of in inception of hotspots.
4. The increase in D/d and decrease in P/d will result in increasing the average values of friction factor and Nusselt number. The change in wire diameter has no significant effect on the average values.
5. Thermal hydraulic performance ratio for the wrapped wire annulus is significantly higher than unity.

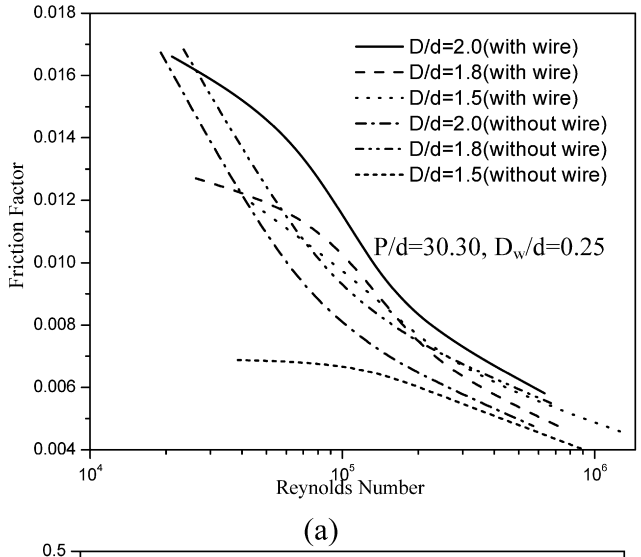

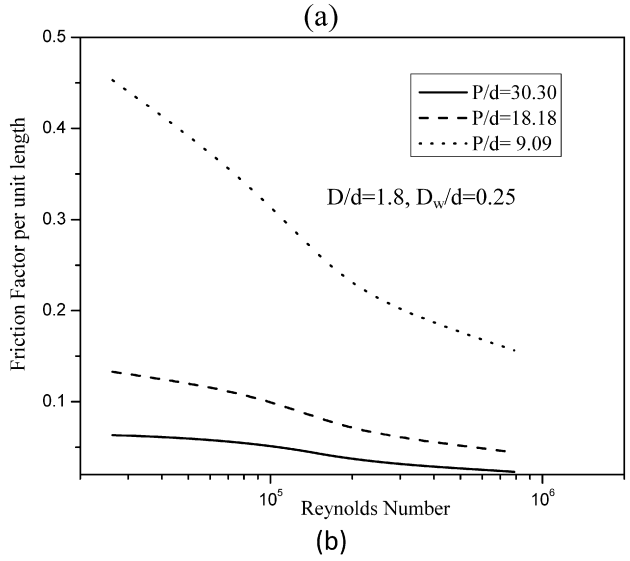

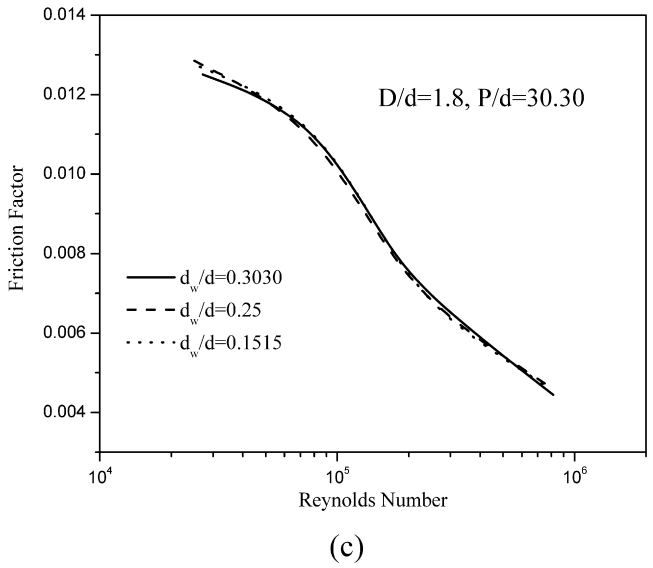

Fig. 22. Friction factor variation for various (a) D/d, (b) P/d, (c) D_W/d.

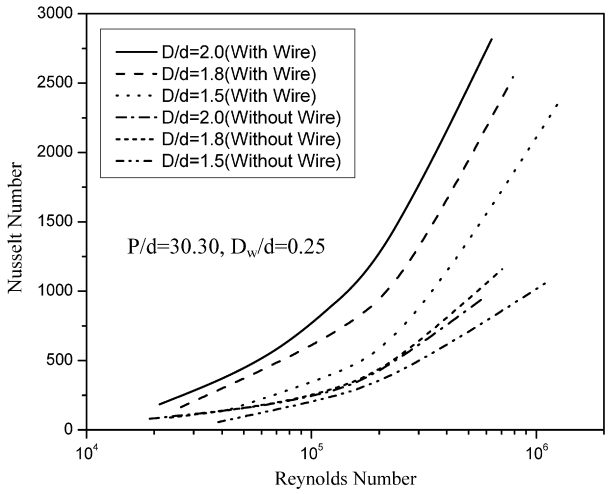

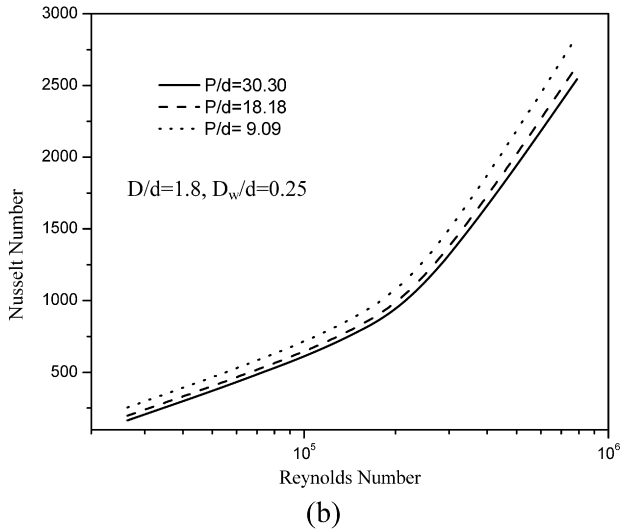

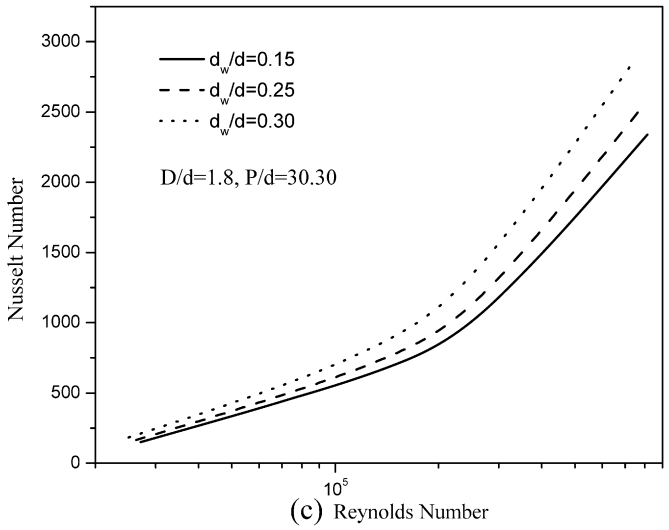

Fig. 23. Nusselt number variation for various (a) D/d, (b) P/d, (c) D_W/d.

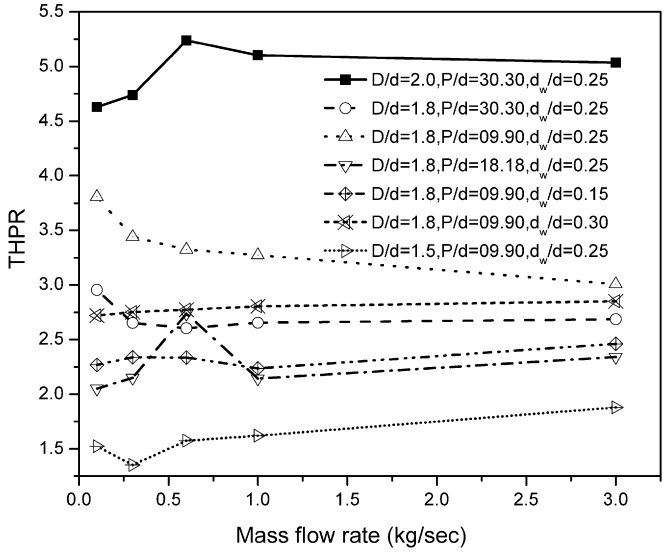

Fig. 24. Variation of THPR with mass flow rate for various configurations.

Acknowledgements

The authors gratefully acknowledge the financial assistance received from the Indira Gandhi Center for Atomic Research, Govt. of India – IIT Madras project.

References

[1] F.M. White, Fluid Mechanics, fourth edition, McGraw-Hill, New York, 1999.
[2] F.W. Dittus, L.M.K. Boelter, Publications on Engineering, vol. 2, University of California, Berkeley, 1930, p. 443.
[3] A.S. Foust, G.A. Christian, Non-boiling heat transfer co-efficients in annuli, American Institute of Chemical Engineers 36 (1940) 541–554.
[4] E.S. Davis, Heat transfer and pressure drop in annuli, Trans. ASME (1943) 755–760.
[5] R.P. Stein, W. Begell, Heat transfer to water in turbulent flow in internally heated annuli, American Institute of Chemical Engineers Journal 4 (2) (1958) 127–131.
[6] W.M. Kays, E.Y. Leung, Heat transfer in annular passages-hydrodynamically developed turbulent flow with arbitrarly prescribed heat flux, Int. J. Heat Mass Transfer 6 (1963) 537–557.
[7] H. Barrow, Y. Lee, A. Roberts, The similarity hypothesis applied to turbulent flow in an annulus, Int. J. Heat Mass Transfer 8 (1965) 1499–1505.
[8] C.A. Sleicher, M.W. Rouse, A convenient correlation for heat transfer to constant and variable property fluids in turbulent pipe flow, Int. J. Heat and Mass Transfer 18 (1975) 677–683.
[9] J. Dirker, J.P. Meyer, Convective heat transfer coefficients in concentric annuli, Heat Transfer Engrg. 26 (2) (2005) 38–44.
[10] P. Kumar, R.L. Judd, Heat transfer with coiled wire turbulence promoters, Can. J. Chem. Engrg. 48 (1970) 378–383.
[11] D.L. Gee, R.L. Webb, Forced convection heat transfer in helically rib-roughned tubes, Int. J. Heat Mass Transfer 23 (1980) 1127–1136.
[12] R. Sethumadhavan, A. Raja Rao, Turbulent flow heat transfer and fluid friction in helical wire inserted tubes, Int. J. Heat Mass Transfer 26 (1983) 1833–1845.
[13] S.K. Saha, U.N. Gaitonde, A.W. Date, Heat transfer and pressure drop characteristics of laminar flow in a circular tube fitted with regularly spaced twisted-tape elements, Exp. Therm. Fluid Sci. 23 (1989) 310–322.
[14] S. Eiamsa-ard, P. Promovonge, Heat transfer characteristics in a tube fitted with helical screw-tape with/without core-rod inserts, Int. Comm. Heat and Mass Transfer 34 (2) (2007) 176–185.
[15] H. Gül, D. Evinb, Heat transfer enhancement in circular tubes using helical swirl generator insert at the entrance, Int. J. Thermal Sci. 46 (2007) 1297–1303.
[16] F.R. Menter, Two-equation eddy-viscosity turbulence models for engineering applications, AIAA Journal 32 (1994) 269–289.
[17] J.F. Fan, W.K. Ding, J.F. Zhang, Y.L. He, W.Q. Tao, A performance evaluation plot of enhanced heat transfer techniques, Int. J. Heat Mass Transfer 52 (1–2) (2008) 33–44.